

Improving robustness of jet tagging algorithms with adversarial training

Annika Stein¹  · Xavier Coubez^{1,2}  · Spandan Mondal¹  · Andrzej Novak¹  · Alexander Schmidt¹ 

Abstract Deep learning is a standard tool in the field of high-energy physics, facilitating considerable sensitivity enhancements for numerous analysis strategies. In particular, in identification of physics objects, such as jet flavor tagging, complex neural network architectures play a major role. However, these methods are reliant on accurate simulations. Mismodeling can lead to non-negligible differences in performance in data that need to be measured and calibrated against. We investigate the classifier response to input data with injected mismodelings and probe the vulnerability of flavor tagging algorithms via application of adversarial attacks. Subsequently, we present an adversarial training strategy that mitigates the impact of such simulated attacks and improves the classifier robustness. We examine the relationship between performance and vulnerability and show that this method constitutes a promising approach to reduce the vulnerability to poor modeling.

Keywords High-energy physics · Deep learning · Jet flavor tagging · Adversarial attacks · Adversarial training · Robustness

1 Introduction

The experiments at the Large Hadron Collider (LHC) at CERN handle large, high-dimensional datasets to find complex patterns or to identify rare signals in background-dominated regions – tasks where machine learning and especially deep learning [1,2] provide considerable performance gains over traditional methods. It

Correspondence to: annika.stein@cern.ch

¹ RWTH Aachen University, Aachen, Germany

² Brown University, Providence, USA

is expected that the relevance of new deep learning technologies will increase, with the era of the High-Luminosity LHC (HL-LHC) approaching [3]. However, studies with the aim of understanding a neural network’s decisions demonstrate the relevance of explainability [4] and raise questions on the safety of systems that use artificial intelligence (AI), which is often perceived as a black-box [4,5]. Moreover, other studies show that small modifications of the inputs (*adversarial examples*) can severely affect the performance of neural networks [6,7] (*adversarial attack*), a worrying prospect for a field that is reliant on simulation, which might be at times inaccurate. Careful exploration of the susceptibility to mismodelings is necessary to examine how severe these “intriguing properties of neural networks” [6] are in practice, which could be driven by the combination of the linear nature of deep neural networks, together with the large number of input variables [6,7]. Applied to computer vision / image recognition, it has been demonstrated that modifications that involve only one pixel are enough to “fool” a neural network [8].

We apply methods from AI safety [5,9,10] to the classification of jets based on the flavor of their initiating particle (a quark or gluon), so called jet heavy-flavor identification (tagging) [11,12]. Identifying the jet flavor plays an important role in various analysis branches exploited by experiments like CMS [11,13] and ATLAS [14,15], for example, for the observation of the decay of the Higgs boson to bottom (b) quark-antiquark pairs ($H \rightarrow b\bar{b}$) [16,17,18]. Moreover, for analyses that also apply charm (c) tagging [11,19,20,21], such as searches for the Higgs boson decaying to c quarks [22,23,24], multiclassifiers become increasingly important. Therefore, investigating the susceptibility to mismodeling could be even more relevant for c tagging. We probe the trade-off between performance and

robustness to systematic distortions by benchmarking an established algorithm for jet flavor tagging with a realistic dataset. Early taggers included only the displacement of tracks as a way to discriminate heavy-from light-flavored jets, possible due to the different lifetimes of the initiating hadrons. It's also possible to leverage information related to the secondary vertices, giving rise to algorithms such as the (deep) combined secondary vertex algorithm [11].

Mismodelings can arise at various steps during the Monte Carlo (MC) simulation chain, starting with the hard process (matrix element calculation), followed by the subsequent steps that model the parton shower, fragmentation and hadronization, where the perturbation order is limited, and ending with the detector simulation [20] which introduces imperfections such as detector misalignment and calorimeter miscalibration.

These imperfections in the modeling, particularly for variables with high discriminating power, demand the calibration of the discriminator shapes [20] and call for investigations of the tagger response to slightly distorted input data [9]. We use adversarial attacks to model systematic uncertainties induced by these subtle mismodelings that could be invisible to typical validation methods, as proposed in Ref. [9]. The approach followed in this study does not eliminate these mismodelings, nor does it provide a definitive *a posteriori* correction, but it helps in estimating to what extent tagging efficiency and misidentification rates could be affected [9, 18]. We assume that more adversarially robust models also generalize better when applied to a non-training domain [2, 25] (e.g. model evaluated on data [9, 20]). To that end, we seek to modify the training to minimize the impact of adversarial attacks, without sacrificing performance. Using *adversarial training* [25, 26, 27] to decrease the effect of simulation-specific artefacts, we show that the injection of systematically distorted samples during the training yields a successful defense strategy. In related works, adversarial training is employed through joint training of a classifier and an adversary [28], making use of gradient reversal layers to connect two networks or by utilizing domain adaptation [29, 30, 31, 32]. Other approaches towards regularization and generalization in the realm of high-energy physics include data augmentation or uncertainty-aware learning [33].

2 Dataset and input features

We use the JET FLAVOR DATASET [12]. These samples are generated with MADGRAPH5 [34] and PYTHIA 6 [35]. The detector response is simulated with DELPHES 3 [36], using the ATLAS [14] detector configuration.

Jets are clustered with the anti- k_T algorithm [37] using the FASTJET [38] package, with $R = 0.4$. Secondary vertices are reconstructed using the adaptive vertex reconstruction algorithm, as implemented in RAVE [39]. Parton matching within a cone of $\Delta R < 0.5$ is used to define the simulated truth labeling of jets. The targets fall in one of the three classes, depending on the jet flavor: light (up, down, strange quarks or gluons), charm, or bottom [12], where the flavor content is distributed among the classes as 48.7% : 12.0% : 39.3%.

2.1 Input features

A description of all input variables is given in Tables 1 and 2, and is based on Ref. [12]; here we only summarize the main categorization.

Input features are organized hierarchically. Low-level features consist of tracks and their helix parameters, along with the track covariance matrix. Additional information is taken from the relationship between each track and the associated vertex. Up to 33 tracks, sorted by impact parameter significance, are available per jet, however, we only consider the first six.

At jet level, expert (high-level) features are constructed as a function of the low-level inputs, for example by summing over all tracks or summing over secondary vertices, such as the weighted sum of displacement significances. Additionally, kinematic features of the jet are taken into account.

Missing or otherwise unavailable variables are filled with a convenient default value for later processing.

2.2 Preprocessing

The entire dataset consists of 11491971 jets, which are split randomly into training (72%), validation (8%) and test (20%) sets. Input features are normalized such that they have a mean of 0 and standard deviation of 1. The scaling is calculated only using the training dataset distributions, excluding the defaulted values. Defaulted input values are set just below the minima of the primary input distributions ensuring no interference between regular and irregular (or missing) values. Minimizing the gap between the default value to the rest of the distributions improves training convergence. This technique of missing data imputation allows us to create fixed length input shapes that are transferred to the first layer of a deep feed-forward neural network, and at the same time prevents vanishing or exploding gradients due to extreme values for the defaults [2, 40, 41].

Sample weights are calculated in order to exclude a potential flavor dependence of the classifier on the particular kinematic properties of the chosen dataset and to correct for the inherent class imbalance. The reweighting aims at identical, kinematic distributions for all three flavors and is done with respect to the jet transverse momentum (p_T) and pseudorapidity (η) distributions [11]. The target shape is the average of the three initial distributions. These are binned into a 2D grid of 50×50 bins, spanning ranges between (20, 900) GeV and $(-2.5, 2.5)$, respectively. When calculating the loss per batch, these weights are multiplied to the individual losses per sample.

3 Methods

3.1 Reference classifier

The studies are carried out on a jet flavor tagging algorithm similar in implementation to the ones used at the LHC experiments, such as ATLAS and CMS. We use a fully-connected sequential model with five hidden layers of 100 nodes each. We use dropout layers [42] with a 10% probability of zeroing out each neuron at each hidden layer to prevent overfitting. The Rectified Linear Unit (ReLU) activation function [2, 40, 11] is used for the hidden layers, the activation of the output layer is computed with the Softmax [2, 11] function. In total, there are 184 input nodes, where the low-level per track features are flattened. We define three output classes, analogous to the dataset.

As loss function, we use the categorical cross entropy loss [40, 43], multiplied with an additional term that downweights easy-to-classify samples during training. In a setting with highly-imbalanced data this ensures smooth classifier output distributions. This method is called focal loss [44, 45] and we use a focusing parameter of $\gamma = 25$.

Model parameters are updated with the Adaptive Moments Estimation (Adam) optimizer [46] using PyTorch's [47] default settings, which is further controlled with a learning rate schedule [48] that starts at 0.0001 and decays proportionally to $\left(1 + \frac{\text{epoch}}{30}\right)^{-1}$. The batch size has been fixed to $2^{16} = 65536$. To ensure that there is no overfitting, training is stopped when the validation loss no longer improves [2]. For each training, the model's parameters are saved after each iteration through the full training dataset (i.e. after each epoch) to store a checkpoint for later evaluation.

3.2 Evaluation metrics

While multi-class taggers are convenient for implementation, for physics analysis purposes one is often interested in constructing classifiers distinguishing two classes at a time. We take appropriate likelihood ratios of the bottom, charm and light output classes as needed for discrimination. The likelihood ratio $XvsY$ for discriminating class X from Y is given as:

$$\frac{P(X)}{P(X) + P(Y)}. \quad (1)$$

For example, for the BvsL discriminator, $P(X)$ and $P(Y)$ refer to the classifier's score for the bottom and light flavor jets, respectively. The performance of the binary classifiers is visualized and evaluated using Receiver Operating Characteristic (ROC) curves [49, 50, 51]. With some loss of information, a ROC curve is characterized by its area under the curve (AUC), which can be used as a reasonable single scalar proxy for the classifier performance [52]. It should be noted that due to a large class imbalance in the available dataset, generic measures like accuracy could be an inaccurate measure of the performance [52].

3.3 Adversarial attacks

One way to generate adversarial inputs is the Fast Gradient Sign Method (FGSM) [2, 7], which modifies the inputs in a systematic way, such that the loss function increases. First, the direction of the steepest increase of the loss function around the raw inputs is computed. Mathematically, the operator that allows to retrieve the “steepest increase” is the gradient of the loss function with respect to the inputs. Once the direction is known, of which only the sign is kept, this vector is multiplied with a (small) limiting parameter ϵ to specify the desired severity of the impact. Then, the nominal inputs are shifted by this quantity. It can, therefore, be seen as a technique to maximally disturb the inputs or maximally confuse the network without necessarily manifesting in the input variable distributions.

Expressed in a single equation, the FGSM attack generates adversarial inputs x_{FGSM} from raw inputs x_{raw} by computing

$$x_{\text{FGSM}} = x_{\text{raw}} + \epsilon \cdot \text{sgn}(\nabla_{x_{\text{raw}}} J(x_{\text{raw}}, y)), \quad (2)$$

where $\text{sgn}(\alpha)$ stands for the sign of α . In Eq. (2), the loss function is denoted as $J(x_{\text{raw}}, y)$, a function of the inputs (x_{raw}) and targets (y). Moreover, the FGSM attack can be interpreted as a method that locally inverts the approach of gradient descent by performing a gradient ascent with the loss function, but in the input

space [7, 25, 27]. Using the terminology of Ref. [25], this is a white box attack with full knowledge of the network (architecture and parameters).

The corresponding visualization is shown in Fig. 1, however, for didactic reasons with one input variable x_i only. In practice, this method is applied multidimensionally, assigning the same limiting parameter ϵ in each input dimension.

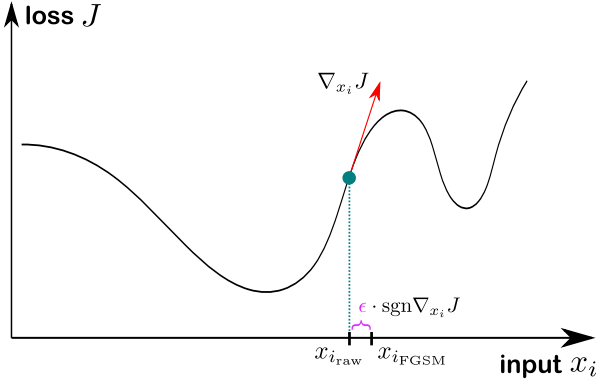


Fig. 1 Visualization of the generation of adversarial inputs by applying the FGSM attack.

Whereas the gradient of an arbitrary function could yield any value, the distortion should stay in reasonable bounds to mimic the behaviour of possible mismodelings or differences between data and simulation [7, 9]. Therefore, we go only a small step in the direction of the gradient, which is expected to introduce practically unnoticeable changes of the input distributions [6, 7].

Increasing the number of inputs to the model also increases the susceptibility towards adversarial attacks, because each shift by ϵ for additional features is propagated to the change in activation [7]. Thus it is conceivable that individual feature distributions remain almost unaffected, but the performance of the neural network is substantially deteriorated.

The FGSM attack does not necessarily replicate a global worst-case scenario [27]. Depending on the actual properties of the loss surface, the adversarial attack could shift the inputs also into local minima (or at least harmless regions), if the limiting parameter is chosen unluckily. On average, with small distortions only, it is still expected that in a given region, the attack will maximally confuse the model up to first order.

In this implementation, the FGSM attack is not applied to integer variables, such as the number of tracks, and defaulted values, which would not be shifted by ϵ in a physically meaningful way.

As large distortions of input variables would be easy to detect, a limit of 25% with respect to the original value is applied on the perturbation. The modified value

x_{FGSM} is then given by Eq. 3, where x denotes the original input value, x' the transformed (preprocessed) value and ϵ the FGSM scaling factor. Inverting the normalization is denoted by $(\cdot)^{-1}$.

$$x_{\text{FGSM}} = \left(x + \text{sgn}(\nabla_x J(x, y)) \cdot \min \left\{ \left| (x' + \text{sgn}(\nabla_x J(x, y)) \cdot \epsilon)^{-1} - x \right|, |0.25 \cdot x| \right\} \right)' \quad (3)$$

3.4 Adversarial training

The approach that will be followed in this study is a simple type of adversarial training that injects perturbed inputs already during the training phase [25]. The algorithmic description is shown in Fig. 2. The difference to the nominal and adversarial training is highlighted in red. In fact, in this approach the neural network never sees the raw inputs during the whole training step [25, 26, 27]. In Fig. 3, this is shown with the insertion of a red block prior to backpropagation. The idea is that by applying the FGSM attack continuously to the training data (for every minibatch, i.e. with every intermediate state of the model after updating the model parameters), the network is less likely to learn the simulation-specific properties of the used sample. Instead, the introduction of a saddle point into the loss surface is expected to improve the generalization capability of the network [2, 25].

Madry et al. [27] have shown that this is an effective method to reduce susceptibility to first-order adversaries, obtained from an FGSM attack. In that sense, adversarial training could also be described as a regularization technique, but a more systematic one than only randomly smearing inputs (another example of data augmentation), randomly deleting connections (dropout), or assigning a probability to the different targets to be wrong (label smoothing) [2].

The principle behind this technique involves the linearity of neural networks to which the high susceptibility to mismodelings is attributed. Adversarial training can be interpreted as a method that adjusts the loss surface to be locally constant around the inputs and that downsizes the impact of perturbations evaluated with a high-dimensional linear function [2]. Slightly distorted inputs then cannot significantly increase the value of the loss function, because it is almost flat in the vicinity of the raw inputs [53]. This can be seen as a geometrical problem where the loss manifold is flattened [53, 54, 55, 56].

When evaluating this adversarially-trained model with distorted test inputs, the model should be more robust to those modifications and the performance should

FOR N EPOCHS:

SPLIT WHOLE TRAINING SAMPLE INTO MINIBATCHES

FOR EVERY MINIBATCH:

DISTORT INPUTS (= APPLY FGSM) - - -

EVALUATE MODEL (FORWARD)

COMPUTE LOSS (AND APPLY LOSS WEIGHTING)

ACCUMULATE GRADIENTS OF LOSS (BACKWARD)

UPDATE MODEL PARAMETERS

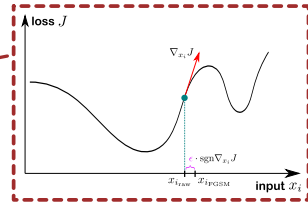


Fig. 2 Adversarial training algorithm. The inputs are distorted prior to the forward and backward passes, with the FGSM attack. The standard training algorithm denoted in black is based on Ref. [40], the modified implementation for adversarial training is demonstrated in Ref. [10].

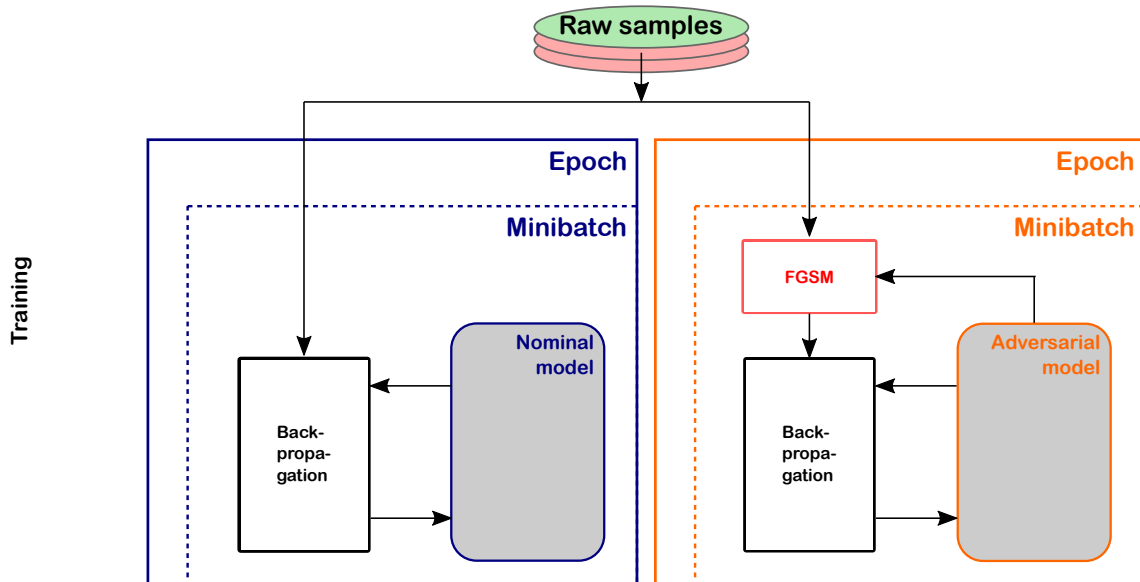


Fig. 3 Comparison of the nominal and adversarial training against the FGSM attack.

not be affected as much as with the generic training. The price for the increased robustness is that the maximally achievable performance on raw inputs can be somewhat reduced with respect to the nominal training [2].

During adversarial training, the FGSM attack uses $\epsilon = 0.01$ when injecting adversarial samples, and no further restrictions are applied, i.e. there is no limitation of the attack with respect to the relative scale of the impact on different values and Eq. 2 holds.

3.5 Inference

The inference step is split into two separate parts, which can be seen in Fig. 4. First, the relevant samples need to be acquired. These can be either original (raw) samples or systematically distorted samples. Both trainings

under consideration have their own respective loss surfaces, which continuously change during the training process. Therefore, samples that maximally deteriorate the performance of one model do not necessarily confuse another model. In order to cause a severe impact, the FGSM attack will be applied individually per training. A similar argument can be made for different checkpoints of the training, where we also craft adversarial samples per epoch to reflect the model's exact status and loss surface. After a fixed number of epochs or after convergence of both training strategies, this yields three different sets of samples: nominal samples (green, equal for both contenders), FGSM samples corresponding to the nominal training (blue), and FGSM samples that have been created for the adversarial training (orange). These can then be injected into the different models for evaluation.

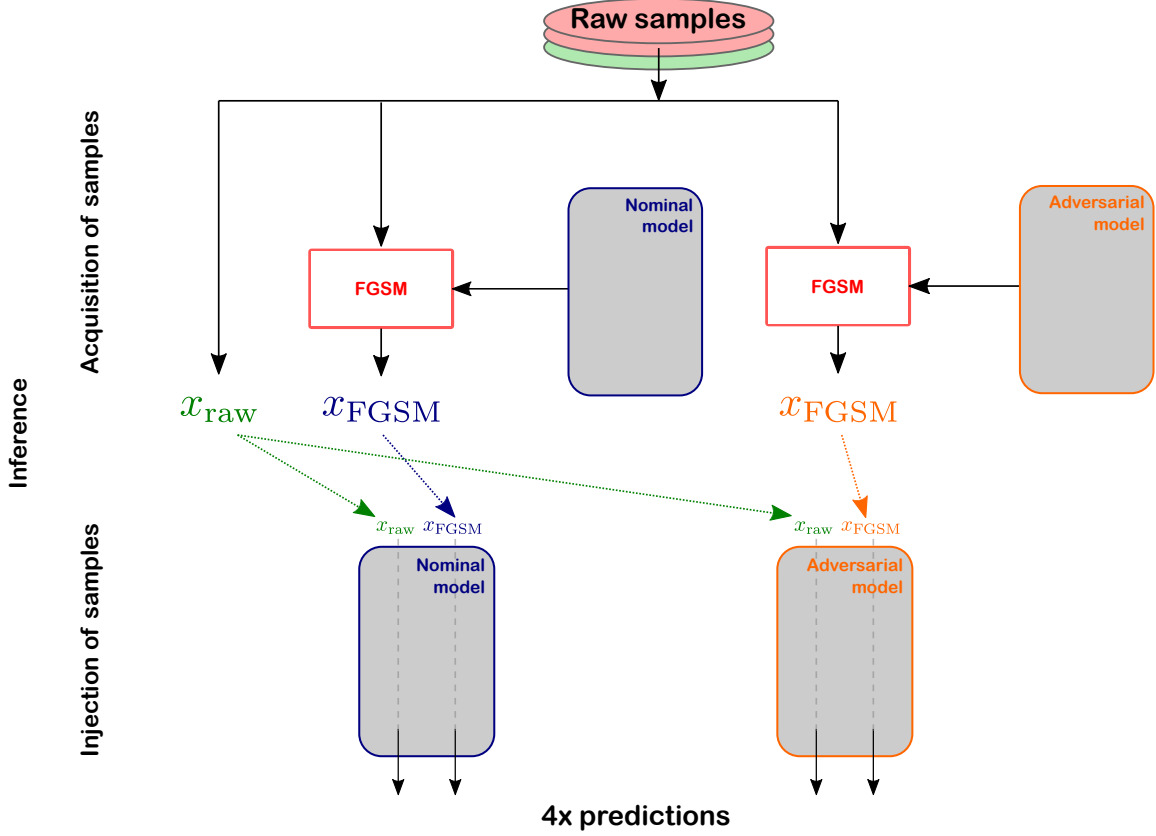


Fig. 4 Schematic overview of the inference process when performing a comparison of robustness of both training strategies. Evaluation of the nominal training (green and blue paths) is described in Sec. 4.2, while the comparison for the adversarial training, including all four combinations is described in Section 4.3.

4 Robustness to mismodeling

4.1 Adversarial attack

As we are interested in producing disturbances that would simulate the behaviour of systematic uncertainties and data-MC disagreement, we verify that the distorted distributions still appear physical. The effect of the FGSM attack at two values of ϵ compared to the nominal distribution is shown for four input variables (both high and low-level inputs) in Fig. 5.

Even with the largest value of $\epsilon = 0.05$ chosen for the following performance studies, the modifications of input shapes remain marginal, within typical data-MC agreements of the level of 10–20% [11].

4.2 Vulnerability of the nominal training

First we establish how susceptible the nominal model is to the FGSM attack (mismodeling) of various magnitudes. Figure 6 shows the ROC curves for the BvsL

(left) and CvsL (right) discriminators, on FGSM datasets generated with varying parameter ϵ and on the nominal inputs. As expected, the model performs best on undisturbed test samples with AUC of 0.946, but the performance decays quite quickly with increasing ϵ . At $\epsilon = 0.05$, which still only causes barely visible differences in the input distributions, the model reaches AUC of 0.883. At 1% mistag working point, this would correspond to a decrease in signal efficiency from 73% to 60%, requiring a scale factor of 0.82.

In the context of the ongoing hunt for better performing classifiers, it is of interest to investigate the susceptibility in relation to the performance. Some insight can be gleaned by evaluating the performance of the classifier at various steps during the training on both the nominal and the perturbed datasets with a fixed $\epsilon = 0.05$, where an AUC value is calculated for each checkpoint. This dependence is shown in Figure 7, again for the two discriminators. Not surprisingly, before the training performance becomes saturated, longer training leads to an increase in nominal performance. However, at the same time it shows higher vulnerability

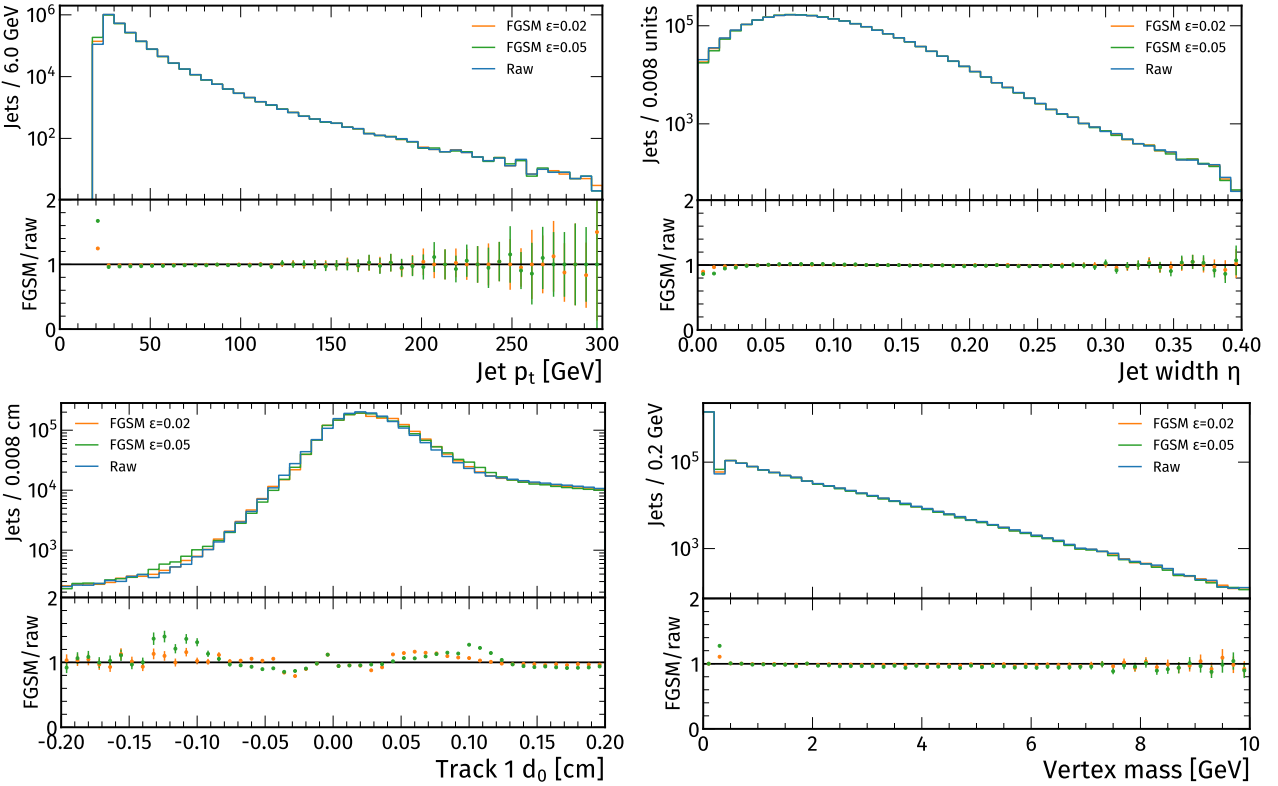


Fig. 5 Distributions of raw and systematically distorted inputs, for a set of features containing high- and low-level information. The displayed range for the signed impact parameter (d_0) of the first track has been clipped to the most relevant central region, where distortions naturally appear enhanced.

towards adversarial attacks. In fact the performance on the perturbed datasets follows exactly the opposite trend. Another way to phrase this finding is that the least performant configuration (after only few epochs or iterations through the full training dataset) shows the highest robustness, i.e. the gap between dashed and solid lines is minimal.

4.3 Improving robustness through adversarial training

In this subsection, the studies described above are repeated with the adversarial model, using the same setup for the attacks when performing the inference.

As a check of robustness, we perform a direct comparison of the nominal and adversarial training, crafting the FGSM samples individually per model, with the resulting ROC curves for the BvsL and CvsL discriminators shown in Fig. 8. The corresponding AUC values for BvsL are identical (0.946) and are practically identical for CvsL (nominal: 0.759, adversarial training 0.757). At the same time, the adversarial model maintains a high performance also when given systematically distorted samples, which can be seen from the dashed-dotted lines corresponding to the colors men-

tioned above. The ROC curve corresponding to FGSM samples crafted for and injected to the adversarial training (orange dashed-dotted line) appears much closer to that showing nominal performance (solid line) than what can be observed for the ROC curves corresponding to the FGSM attack for the nominal training (blue lines). In numbers, this effect is best observed for the CvsL discriminator where the decrease in performance is roughly 21% for the nominal training, but only 8.2% for the adversarial training, while the nominal performance of both models is nearly same. Hence, we have shown that it is possible to build a more robust tagger that is simultaneously highly performant. A label leaking effect (see Ref. [57]), which refers to a better performance on adversarial examples than on undisturbed data for an adversarial model, is not observed.

Figure 9 compares the susceptibility to mismodeling of the two classifiers as a function of performance. FGSM samples have been generated individually for each model and checkpoint (denoting each epoch with a single point) to scan over different discrete stages of the training. Higher density of points in the high performance region is representative of the small improvements at later stages of the training, while the performance gain during the first few epochs is quick.

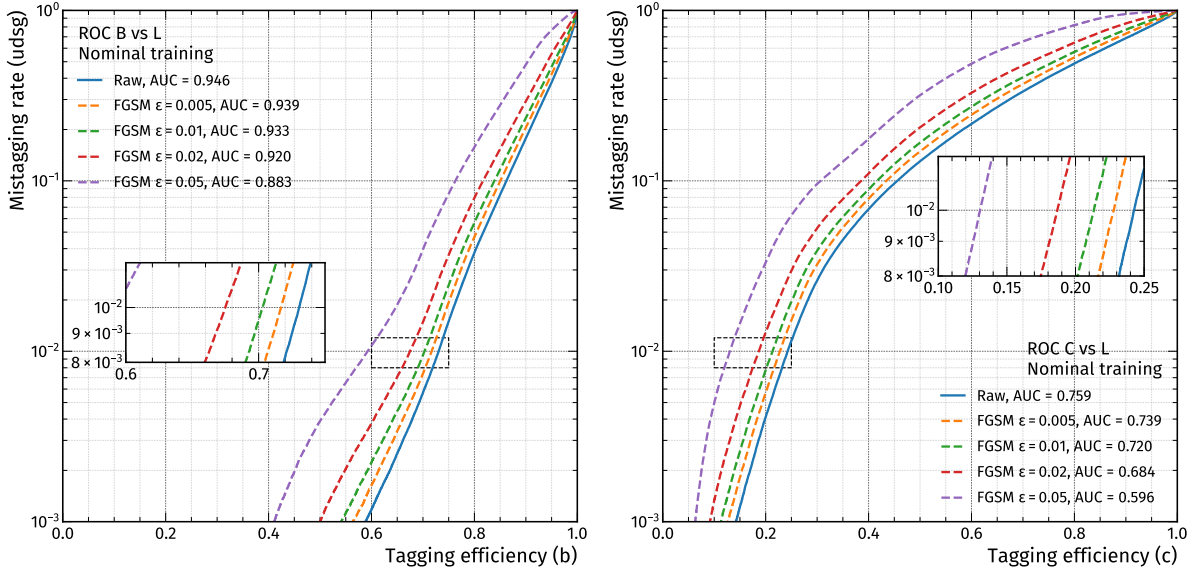


Fig. 6 ROC curves for the BvsL (left) and CvsL discriminator (right), using the nominal training and applying FGSM attacks of different magnitudes. The model is evaluated when the training has reached peak performance.

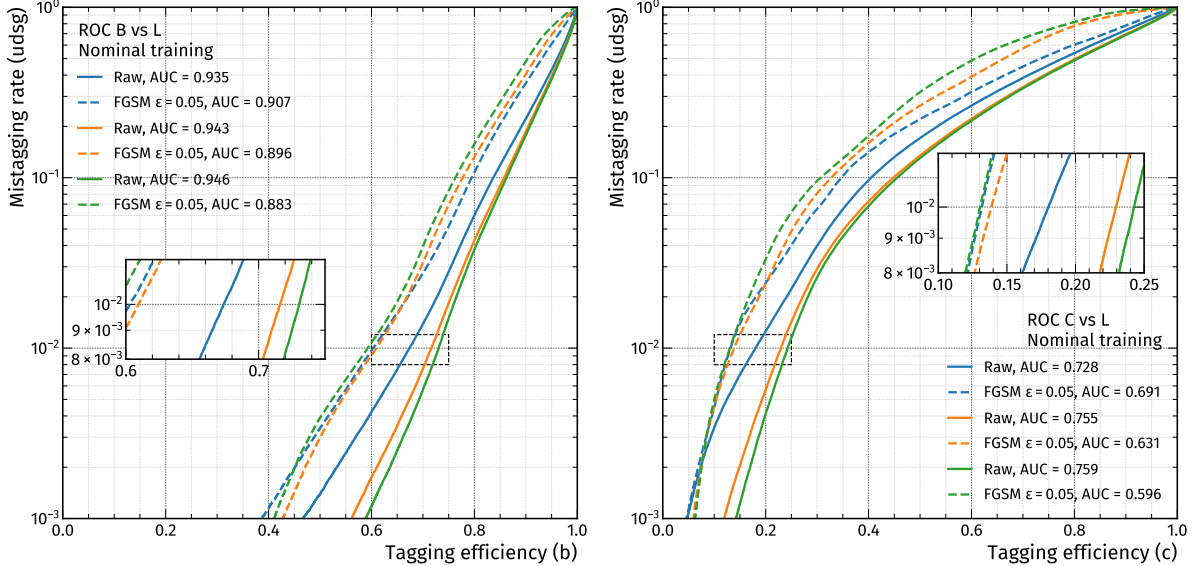


Fig. 7 ROC curves for the BvsL (left) and CvsL discriminator (right), using the nominal training and applying FGSM attacks with $\epsilon = 0.05$ at various checkpoints of the training that each come with different nominal performance. Solid lines in different colors represent nominal performance gain with an increased number of epochs, dashed lines show corresponding performance on individually crafted FGSM samples for the particular checkpoints.

Ideally, there would be a constant relation that shows no signs of decreasing robustness for increasing performance. However, we observe a considerable deterioration (and thus higher susceptibility to miscalibration) of the nominal classifier. The effect for the adversarial model, while still noticeable, is to a large degree mitigated. In fact, the adversarial training seems to recover some of its robustness (e.g. peaking at an AUC of around 0.938) before the impact at higher performance starts to worsen the resistance. Again, this shows

the intriguing trade-off between performance and robustness for the nominal training, where training to highest performance is not necessarily advisable due to high susceptibility. On the other hand, the adversarial training performs equally well on nominal samples and only shows a weak functional dependence between performance on first-order adversaries and the respective undisturbed performance.

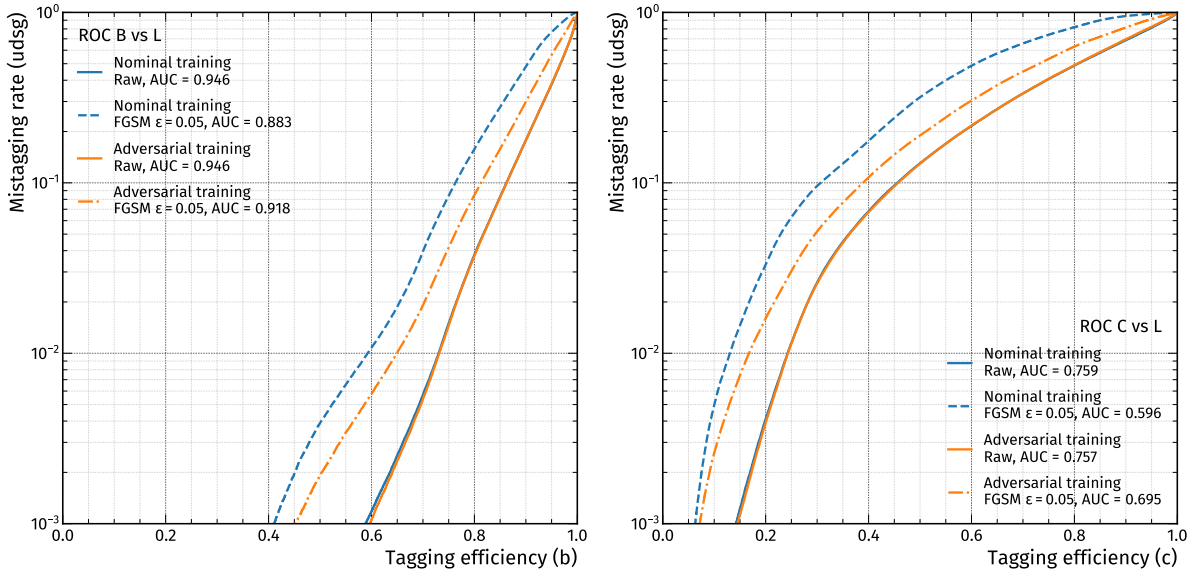


Fig. 8 ROC curves for the BvsL (left) and CvsL (right) discriminators, comparing the nominal with adversarial training when applying the FGSM attack to both trainings individually. Nominal training is visualized in blue, adversarial training in orange, solid lines depict nominal performance, dashed lines show performance on distorted inputs (for nominal training), dashed-dotted lines represent the systematically distorted samples for adversarial training.

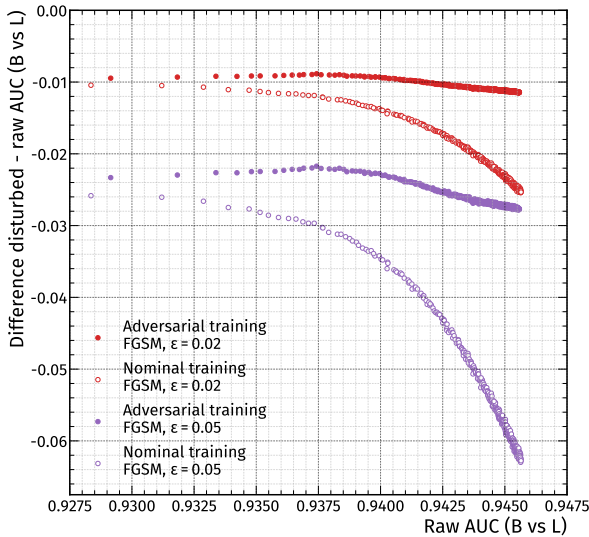


Fig. 9 Relation between susceptibility and nominal performance for the nominal and adversarial training, tested on systematically distorted inputs with varying ϵ in different colors. The x axis shows nominal performance, measured with BvsL AUC, while the y axis shows the difference between disturbed and raw AUC. When there is a drop on the y axis while moving to higher nominal performance (x axis), this indicates higher susceptibility. The empty markers represent the nominal training, which becomes highly vulnerable with increasing nominal performance (with the drop always getting steeper), while the filled markers for adversarial training show a much flatter relation.

4.4 Probing flavor dependence of the attack as a proxy for generalization capability

In an attempt to understand why the adversarial model is more robust than the nominal classifier, we investigate nominal and perturbed input distributions of a selected feature, split by flavor. We intentionally choose a large distortion. This test aims at visualizing geometric properties of the distorted samples, purposefully choosing a large ϵ of 0.1. This is equal to the regular FGSM attack described by Eq. 2 without the limitation described in Eq. 3. The signed impact parameter (d_0) as shown in Fig. 10 originally offers discriminating power via the fact that heavy-flavor jets contain displaced tracks associated to a secondary vertex, which should naturally lead to more positive values for the d_0 variable. For light-flavored jets, this behaviour is not expected, instead the tracks in light jets have a roughly symmetric d_0 distribution, peaking at 0, apart from some skewness due to long-lived hadrons misreconstructed as jets or wrong clustering of tracks from heavy-flavor hadrons into light-flavor jets [11].

For the nominal training, light-flavor jets are shifted mostly into the positive region, which should be dominated by b jets; b jets are shifted to the negative region where these jets were not abundant previously. From a geometric point of view, the FGSM attack on the nominal training produces asymmetric shapes. On the other hand, the resulting perturbed input distributions for the adversarial training are symmetric. We observe that the adversarial model is almost agnostic to the di-

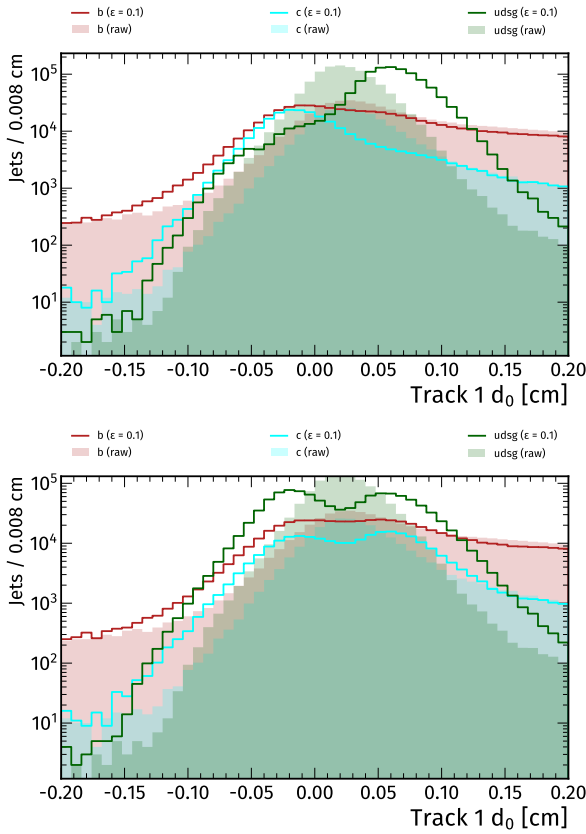


Fig. 10 Signed transverse impact parameter distribution for the first track, split by flavor, before (filled histograms) and after (lines) applying the FGSM attack for the nominal (top) and adversarial (bottom) models, respectively. Clearly asymmetric shapes are produced when using the FGSM attack for the loss function assigned to the nominal training. Applying the FGSM attack based on an adversarial model shows suppressed flavor-dependency and relatively symmetric shapes. The attack uses the parameter $\epsilon = 0.1$, which is higher than the moderately chosen parameter of $\epsilon = 0.01$ during the modified training loop.

rection into which the FGSM attack shifts the inputs, while the nominal training shows a clear preferred direction that could be described as an inversion of the expected physics. For the adversarial training, the attack seems to have difficulties deciding which direction is the worse direction, resulting in a perceived “coin-flipping” of the shift. Thus, the adversarial training remains less susceptible than the nominal training, even when the distortions are noticeably large.

It is conceivable that the different geometric properties of the distributions are related to the geometry of the loss surface [53, 54, 55, 56]. This is expected to be responsible for differences in robustness as well. Figure 11 illustrates how the flatness of the loss surface in the vicinity of raw inputs could influence symmetric or asymmetric shifts.

A nominal training converges into a minimum associated with the default distributions. In that case, for a given flavor, there will be a specific vector pointing away from a local minimum and the direction is fixed according to the steepest increase in loss. The adversarial training always “sees” (new) adversarial inputs, so the adjustment of the model’s parameters might average out eventually over further training epochs. Always following the newly distorted inputs yields a locally constant loss manifold around the original inputs due to the more complex saddle point problem. This would mean that not the exact memorization of training data, but rather higher-order correlations contribute to the improvement of the performance of the adversarial training [25, 27, 53, 54]. With the assumption of a flat loss surface close to the raw inputs there would be no preferred direction for first-order adversarial attacks crafted for the adversarial model. Many vectors would fulfill the criterion of pointing in the direction of increasing loss, much like choosing the direction randomly.

Thus by examining the geometric properties of adversarial samples, a flat loss landscape for the adversarial model is highly probable, leading to higher robustness [53, 54]. For mismodelings of order ϵ that are still on-manifold, the adversarial training would generalize better to data than nominal training. Robustness and generalization are not equivalent [25, 27, 58], which is why the above statement can not be general, but is only valid under the assumption that adversarial methods like the FGSM attack replicate mismodelings between simulation and detector data.

5 Conclusion

In this paper, we investigated the performance of a jet flavor tagging algorithm when being exposed to systematically distorted inputs that have been generated with an adversarial attack, the Fast Gradient Sign Method. Moreover, we showed how model performance and robustness are related. We explored the trade-off between performance on unperturbed and on distorted test samples, investigating ROC curves and AUC scores for the BvsL and CvsL discriminators. All tests conducted with the nominal training confirm earlier findings that relate higher performance with higher susceptibility, now for a deep neural network that replicates a typical jet tagging algorithm. We applied a defense strategy to counter first-order adversarial attacks by injecting adversarial samples already during the training stage of the classifier, but without altering the network architecture.

When comparing this new classifier with the nominal model, no difference in performance was observed,

but the robustness towards adversarial attacks is enhanced by a large margin. Exemplary for the direct comparison of the two trainings, both reached an AUC score of approximately 76% when discriminating c from light jets, but an FGSM attack that is still moderate in its impact on the input distributions decreases the performance of the nominal training by 21%, and only by 8.2% for the adversarial training. A study of raw and distorted input distributions allowed us to relate geometric properties of the attack with geometric properties of the underlying loss surfaces for a nominal and an adversarially trained model, yielding a possible explanation for the higher robustness of the latter attributed to flatness of the loss manifold.

To some extent, the higher robustness as shown in this paper points at better generalization capability, but a study that will also utilize detector data has yet to be conducted to confirm this conjecture. The approach followed for this work is comparatively general, in that it only needs access to the model and the criterion. This is the first application of adversarial training to build a robust jet flavor tagger suitable for usage at the LHC.

It would be interesting to apply this type of attack and defense also to more complex neural network structures to see if, for example, convolutional layers are able to leverage adversarial attacks differently, and if adversarial training is as effective for taggers with a larger (or smaller) dimension in the feature space. Another focus could be targeted at using adversarial methods of higher complexity, both for the attack, as well as for the defense against them. Summarizing the efforts so far, adversarial training was applied successfully to resist first-order adversarial attacks on jet flavor tagging algorithms, corresponding studies with higher-order adversaries are left for future investigations.

Acknowledgements Simulations were performed with computing resources granted by RWTH Aachen University under project `nova0021` and `rwth0619`. This work has received support by the Deutsche Forschungsgemeinschaft (DFG, German Research Foundation, projects SCHM 2796/5 and GRK 2497), and the Bundesministerium für Bildung und Forschung (BMBF, Project 05H2021). We thank Nicolas Frediani for his contributions to the project in context of his Bachelor thesis.

Compliance with ethical standards

Conflict of interest On behalf of all authors, the corresponding author states that there is no conflict of interest.

References

1. Lecun, Y., Bengio, Y., Hinton, G.: Deep learning. *Nat. Cell Biol.* **521**(7553) (2015) 436 <https://doi.org/10.1038/nature14539>.
2. Goodfellow, I., Bengio, Y., Courville, A.: Deep Learning. MIT Press (2016) Online. <http://www.deeplearningbook.org> Accessed 25 Mar 2022.
3. Albertsson, K., Altoe, P., Anderson, D., et al.: Machine Learning in High Energy Physics Community White Paper. *J. Phys. Conf. Ser.* **1085**(2) (2018) 022008 <https://doi.org/10.1088/1742-6596/1085/2/022008> <http://www.arxiv.org/abs/1807.02876> [physics.comp-ph].
4. Adadi, A., Berrada, M.: Peeking Inside the Black-Box: A Survey on Explainable Artificial Intelligence (XAI). *IEEE Access* **6** (2018) 52138–52160 <https://doi.org/10.1109/ACCESS.2018.2870052>.
5. Amodei, D., Olah, C., Steinhardt, J., et al.: Concrete Problems in AI Safety. arXiv preprint <http://www.arxiv.org/abs/1606.06565> [cs.AI] (2016)
6. Szegedy, C., Zaremba, W., Sutskever, I., et al.: Intriguing properties of neural networks. arXiv preprint <http://www.arxiv.org/abs/1312.6199> [cs.CV] (2014)
7. Goodfellow, I.J., Shlens, J., Szegedy, C.: Explaining and Harnessing Adversarial Examples. arXiv preprint <http://www.arxiv.org/abs/1412.6572> [stat.ML] (2015)
8. Su, J., Vargas, D.V., Sakurai, K.: One Pixel Attack for Fooling Deep Neural Networks. *IEEE Transactions on Evolutionary Computation* **23**(5) (Oct 2019) 828–841 <http://dx.doi.org/10.1109/tevc.2019.2890858> <http://www.arxiv.org/abs/1710.08864> [cs.LG].
9. Nachman, B., Shimmin, C.: AI Safety for High Energy Physics. arXiv preprint <https://arxiv.org/abs/1910.08606> [hep-ph] (2019)
10. cshimmin / C. Shimmin: advjets-mlhep2020. GitHub repository. <https://github.com/cshimmin/advjets-mlhep2020> Accessed 25 Mar 2022
11. CMS Collaboration: Identification of heavy-flavour jets with the CMS detector in pp collisions at 13 TeV. *JINST* **13** (2018) P05011 <https://doi.org/10.1088/1748-0221/13/05/P05011> <http://www.arxiv.org/abs/1712.07158> [physics.ins-det].
12. Guest, D., Collado, J., Baldi, P., et al.: Jet flavor classification in high-energy physics with deep neural networks. *Physical Review D* **94**(11) (Dec 2016) <https://doi.org/10.1103/PhysRevD.94.112002> <http://www.arxiv.org/abs/1607.08633> [hep-ex].
13. CMS Collaboration: The CMS Experiment at the CERN LHC. *JINST* **3** (2008) S08004 <https://doi.org/10.1088/1748-0221/3/08/S08004>.
14. ATLAS Collaboration: The ATLAS Experiment at the CERN Large Hadron Collider. *JINST* **3** (2008) S08003 <https://doi.org/10.1088/1748-0221/3/08/S08003>.
15. ATLAS Collaboration: ATLAS b-jet identification performance and efficiency measurement with $t\bar{t}$ events in pp collisions at $\sqrt{s} = 13$ TeV. *Eur. Phys. J. C* **79**(11) (2019) 970 <https://doi.org/10.1140/epjc/s10052-019-7450-8> <http://www.arxiv.org/abs/1907.05120> [hep-ex].
16. CMS Collaboration: Observation of Higgs Boson Decay to Bottom Quarks. *Physical Review Letters* **121**(12) (Sep 2018) <https://doi.org/10.1103/physrevlett.121.121801> <http://www.arxiv.org/abs/1808.08242> [hep-ex].
17. ATLAS Collaboration: Observation of $H \rightarrow b\bar{b}$ decays and VH production with the ATLAS detector.

Phys. Lett. B **786** (2018) 59–86 <https://doi.org/10.1016/j.physletb.2018.09.013> <http://www.arxiv.org/abs/1808.08238> [hep-ex].

18. Kogler, R., Nachman, B., Schmidt, A., et al.: Jet Substructure at the Large Hadron Collider: Experimental Review. Rev. Mod. Phys. **91**(4) (2019) 045003 <https://doi.org/10.1103/RevModPhys.91.045003> <http://www.arxiv.org/abs/1803.06991> [hep-ex].

19. CMS Collaboration: Identification of c-quark jets at the CMS experiment. Online. <https://cds.cern.ch/record/2205149>. Accessed 25 Mar 2022 (2016)

20. CMS Collaboration: A new calibration method for charm jet identification validated with proton-proton collision events at $\sqrt{s} = 13$ TeV. JINST **17** (2022) <https://doi.org/10.1088/1748-0221/17/03/P03014> <http://www.arxiv.org/abs/2111.03027> [hep-ex].

21. ATLAS Collaboration: Measurement of the c-jet mistagging efficiency in $t\bar{t}$ events using pp collision data at $\sqrt{s} = 13$ TeV collected with the ATLAS detector. Eur. Phys. J. C **82**(1) (2022) 95 <https://doi.org/10.1140/epjc/s10052-021-09843-w> <http://www.arxiv.org/abs/2109.10627> [hep-ex].

22. CMS Collaboration: A search for the standard model Higgs boson decaying to charm quarks. JHEP **03** (2020) 131 [https://doi.org/10.1007/JHEP03\(2020\)131](https://doi.org/10.1007/JHEP03(2020)131) <http://www.arxiv.org/abs/1912.01662> [hep-ex].

23. ATLAS Collaboration: Direct constraint on the Higgs-charm coupling from a search for Higgs boson decays into charm quarks with the ATLAS detector. arXiv preprint <https://arxiv.org/abs/2201.11428> [hep-ex] (2022)

24. CMS Collaboration: Direct search for the standard model Higgs boson decaying to a charm quark-antiquark pair. Online. <https://cds.cern.ch/record/2802742> Accessed 25 Mar 2022 (2022)

25. Chakraborty, A., Alam, M., Dey, V., Chattopadhyay, A., Mukhopadhyay, D.: Adversarial Attacks and Defences: A Survey. arXiv preprint <http://www.arxiv.org/abs/1810.00069> [cs.LG] (2018)

26. Shaham, U., Yamada, Y., Negahban, S.: Understanding adversarial training: Increasing local stability of supervised models through robust optimization. Neurocomputing **307** (Sep 2018) 195–204 <http://dx.doi.org/10.1016/j.neucom.2018.04.027> <http://www.arxiv.org/abs/1511.05432> [stat.ML].

27. Madry, A., Makelov, A., Schmidt, L., Tsipras, D., Vladu, A.: Towards Deep Learning Models Resistant to Adversarial Attacks. ICLR’18. arXiv preprint <http://www.arxiv.org/abs/1706.06083> [stat.ML] (2019)

28. Louppe, G., Kagan, M., Cranmer, K.: Learning to Pivot with Adversarial Networks. arXiv preprint <https://arxiv.org/abs/1611.01046> [stat.ML] (11 2016)

29. Ganin, Y., Lempitsky, V.: Unsupervised Domain Adaptation by Backpropagation. arXiv preprint <http://www.arxiv.org/abs/1409.7495> [stat.ML] (2015)

30. CMS Collaboration: A deep neural network to search for new long-lived particles decaying to jets. Machine Learning: Science and Technology **1**(3) (Aug 2020) 035012 <http://dx.doi.org/10.1088/2632-2153/ab9023> <http://www.arxiv.org/abs/1912.12238> [hep-ex].

31. Ćiprijanović, A., Kafkes, D., Snyder, G., et al.: DeepAdversaries: Examining the Robustness of Deep Learning Models for Galaxy Morphology Classification. arXiv preprint <https://arxiv.org/abs/2112.14299> [cs.LG] (12 2021)

32. Babicz, M., Alonso-Monsalve, S., Dolan, S., Terao, K.: Adversarial methods to reduce simulation bias in neutrino interaction event filtering at Liquid Argon Time Projection Chambers. arXiv preprint <http://www.arxiv.org/abs/2201.11009> [hep-ex] (1 2022)

33. Ghosh, A., Nachman, B., Whiteson, D.: Uncertainty-aware machine learning for high energy physics. Physical Review D **104**(5) (Sep 2021) <https://doi.org/10.1103/physrevd.104.056026> <http://www.arxiv.org/abs/2105.08742> [physics.data-an].

34. Alwall, J., Herquet, M., Maltoni, F., Mattelaer, O., Stelzer, T.: MadGraph 5 : Going Beyond. JHEP **06** (2011) 128 [https://doi.org/10.1007/JHEP06\(2011\)128](https://doi.org/10.1007/JHEP06(2011)128) <http://www.arxiv.org/abs/1106.0522> [hep-ph].

35. Sjostrand, T., Mrenna, S., Skands, P.Z.: PYTHIA 6.4 Physics and Manual. JHEP **05** (2006) 026 <https://doi.org/10.1088/1126-6708/2006/05/026> <http://www.arxiv.org/abs/hep-ph/0603175> [hep-ph].

36. de Favereau, J., Delaere, C., Demin, P., et al.: DELPHES 3, A modular framework for fast simulation of a generic collider experiment. JHEP **02** (2014) 057 [https://doi.org/10.1007/JHEP02\(2014\)057](https://doi.org/10.1007/JHEP02(2014)057) <http://www.arxiv.org/abs/1307.6346> [hep-ex].

37. Cacciari, M., Salam, G.P., Soyez, G.: The anti- k_t jet clustering algorithm. JHEP **2008**(04) (Apr 2008) 063–063 <https://doi.org/10.1088/1126-6708/2008/04/063> <http://www.arxiv.org/abs/0802.1189> [hep-ph].

38. Cacciari, M., Salam, G.P., Soyez, G.: FastJet User Manual. Eur. Phys. J. C **72** (2012) 1896 <https://doi.org/10.1140/epjc/s10052-012-1896-2> <http://www.arxiv.org/abs/1111.6097> [hep-ph].

39. Waltenberger, W.: RAVE: A detector-independent toolkit to reconstruct vertices. IEEE Trans. Nucl. Sci. **58** (2011) 434–444 <https://doi.org/10.1109/TNS.2011.2119492>.

40. Stevens, E., Antiga, L., Viehmann, T.: Deep learning with PyTorch. Manning Publications Company (2020)

41. Kuhn, M., Johnson, K.: Feature Engineering and Selection: A Practical Approach for Predictive Models. Chapman & Hall/CRC Data Science Series. CRC Press (2019)

42. Srivastava, N., Hinton, G., Krizhevsky, A., Sutskever, I., Salakhutdinov, R.: Dropout: A Simple Way to Prevent Neural Networks from Overfitting. Journal of Machine Learning Research **15**(1) (2014) 1929–1958 Online. <https://jmlr.org/papers/volume15/srivastava14a/srivastava14a.pdf> Accessed 25 Mar 2022.

43. PyTorch: CrossEntropyLoss. Online. <https://pytorch.org/docs/stable/generated/torch.nn.CrossEntropyLoss.html> Accessed 25 Mar 2022

44. Lin, T.Y., Goyal, P., Girshick, R., He, K., Dollár, P.: Focal Loss for Dense Object Detection. In: 2017 IEEE International Conference on Computer Vision (ICCV). (2017) 2999–3007 <https://doi.org/10.1109/ICCV.2017.324> <http://www.arxiv.org/abs/1708.02002> [cs.CV].

45. AdeelH / A. Hassan: Multi-class Focal Loss. GitHub repository. <https://github.com/AdeelH/pytorch-multi-class-focal-loss> Accessed 25 Mar 2022

46. Kingma, D.P., Ba, J.: Adam: A Method for Stochastic Optimization. In: 3rd International Conference for Learning Representations (ICLR). (2015) arXiv preprint <http://www.arxiv.org/abs/1412.6980> [cs.LG].

47. Paszke, A., Gross, S., Massa, F., et al.: PyTorch: An Imperative Style, High-Performance Deep Learning Library. In: Advances in Neural Information Processing

Systems 32. arXiv preprint <http://www.arxiv.org/abs/1912.01703> [cs.LG]. Curran Associates, Inc. (2019) 8024–8035 NeurIPS 2019.

48. Darken, C., Chang, J., Moody, J.: Learning rate schedules for faster stochastic gradient search. In: Neural Networks for Signal Processing II Proceedings of the 1992 IEEE Workshop. (1992) 3–12 <https://doi.org/10.1109/NNSP.1992.253713>.

49. Davis, J., Goadrich, M.: The Relationship between Precision-Recall and ROC Curves. In: Proceedings of the 23rd International Conference on Machine Learning. ICML '06, New York, NY, USA, Association for Computing Machinery (2006) 233–240 <https://doi.org/10.1145/1143844.1143874>.

50. Powers, D.: Evaluation: From Precision, Recall and F-Factor to ROC, Informedness, Markedness & Correlation. arXiv preprint <https://arxiv.org/abs/2010.16061> [cs.LG] (2020)

51. Galar, M., Fernandez, A., Barrenechea, E., Bustince, H., Herrera, F.: A Review on Ensembles for the Class Imbalance Problem: Bagging-, Boosting-, and Hybrid-Based Approaches. IEEE Transactions on Systems, Man, and Cybernetics, Part C (Applications and Reviews) **42**(4) (2012) 463–484 <https://doi.org/10.1109/TSMCC.2011.2161285>.

52. Branco, P., Torgo, L., Ribeiro, R.P.: A Survey of Predictive Modeling on Imbalanced Domains. ACM Comput. Surv. **49**(2) (August 2016) <https://doi.org/10.1145/2907070> [http://www.arxiv.org/abs/1505.01658](https://www.arxiv.org/abs/1505.01658) [cs.LG].

53. Fawzi, A., Moosavi-Dezfooli, S.M., Frossard, P.: Robustness of classifiers: from adversarial to random noise. Accepted to NIPS 2016. arXiv preprint <http://www.arxiv.org/abs/1608.08967> [cs.LG] (2016)

54. Fawzi, A., Fawzi, O., Frossard, P.: Analysis of classifiers’ robustness to adversarial perturbations. Machine learning **107**(3) (2018) 481–508 <http://dx.doi.org/10.1007/s10994-017-5663-3> [http://www.arxiv.org/abs/1502.02590](https://www.arxiv.org/abs/1502.02590) [cs.LG].

55. Li, H., Xu, Z., Taylor, G., Studer, C., Goldstein, T.: Visualizing the Loss Landscape of Neural Nets. NIPS 2018. arXiv preprint <http://www.arxiv.org/abs/1712.09913> [cs.LG] (2018)

56. Fort, S., Hu, H., Lakshminarayanan, B.: Deep Ensembles: A Loss Landscape Perspective. arXiv preprint <http://www.arxiv.org/abs/1912.02757> [stat.ML] (2020)

57. Kurakin, A., Goodfellow, I., Bengio, S.: Adversarial Machine Learning at Scale. arXiv preprint <http://www.arxiv.org/abs/1611.01236> [cs.CV] (2017)

58. Stutz, D., Hein, M., Schiele, B.: Disentangling Adversarial Robustness and Generalization. 2019 IEEE/CVF Conference on Computer Vision and Pattern Recognition (CVPR) (2019) 6969–6980 <https://doi.org/10.1109/CVPR.2019.00714> [http://www.arxiv.org/abs/1812.00740](https://www.arxiv.org/abs/1812.00740) [cs.CV].

59. dguest / D. Guest: delphes-rave. GitHub repository. <https://github.com/dguest/delphes-rave> Accessed 25 Mar 2022

60. Pivarski, J., Das, P., Osborne, I., et al.: scikit-hep/awkward-1.0: 0.4.5. Zenodo (2020) <https://doi.org/10.5281/zenodo.4341376>.

61. Gray, L., Smith, N., Novak, A., et al.: CoffeaTeam/coffea: Release v0.6.46. Zenodo (2020) <https://doi.org/10.5281/zenodo.3266454>.

62. Hunter, J.D.: Matplotlib: A 2D graphics environment. Computing in Science & Engineering **9**(3) (2007) 90–95 <https://doi.org/10.1109/MCSE.2007.55>.

63. ATLAS Collaboration: Impact parameter-based b-tagging algorithms in the 7 TeV collision data with the ATLAS detector: the TrackCounting and JetProb algorithms. Online. <https://cds.cern.ch/record/1277681> Accessed 25 Mar 2022 (2010)

A Computing

The dataset can be accessed at the UCI Machine Learning in Physics Web portal via <http://mlphysics.ics.uci.edu/> with code accessible under Ref. [59].

Processing of the data is carried out with the `awkward` [60] package, later evaluation is facilitated by utilizing `coffea` [61], the graphics are prepared with `matplotlib` [62]. The neural network training is performed with the PyTorch [47] library, where a NVIDIA Tesla V100 GPU is utilized.

B Supplementary material

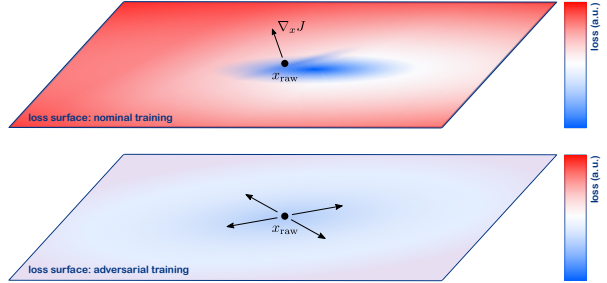


Fig. 11 Illustration of the potential geometry of the loss surfaces for the nominal as well as the adversarial training. Inspired by Refs. [55, 54, 53]

C Input variables

Table 1 Expert / high-level features for the neural network. Horizontal lines separate high-level jet, high-level track and high-level vertex variables. Adapted from Refs. [12, 59].

Short name	Description
Jet p_T	transverse momentum of the jet with respect to the beam line
Jet η	jet pseudorapidity
Track 2 (3) d_0 (z_0) significance	magnitude of impact parameter significance of the second (third) track, transverse to the (along the) beam line, after ranking them by $ d_0 $ significance
N tracks over d_0 threshold	number of tracks with transverse impact parameter significance over 1.8
Jet Prob	light jet probability (see Ref. [63]); product of likelihoods over all tracks to have come from a light quark jet
Jet width η (ϕ)	width of the jet in η (ϕ) coordinates, obtained from all tracks in the jet via
	$\left(\frac{\sum_i p_{T,i} \Delta \eta_i^2}{\sum_i p_{T,i}} \right)^{1/2} \quad \left(\text{or} \left(\frac{\sum_i p_{T,i} \Delta \phi_i^2}{\sum_i p_{T,i}} \right)^{1/2} \right) \quad \text{with respect to the jet axis}$
Vertex significance	weighted sum over displacement significances for all secondary vertices in the jet
	$\frac{\sum_i d_i / \sigma_i^2}{\sqrt{\sum_i 1 / \sigma_i^2}}$
N secondary vertices	number of reconstructed secondary vertices in the jet
N secondary vertex tracks	number of tracks associated to a secondary vertex, summed over all secondary vertices in the jet
Vertex ΔR	sum of angular separation between the secondary vertices and the jet, weighted by the number of tracks at the SV
	$\frac{1}{\sum_i \text{SV}_i \cdot \text{nTracks}} \sum_i \text{SV}_i \cdot \text{nTracks} \cdot \Delta R(\text{Jet}, \text{SV}_i)$
Vertex mass	decay chain mass, i.e. sum over all secondary vertex masses in the jet, under the pion mass hypothesis for reconstructed particles
Vertex energy fraction	summed fractions of total track energy in the jet associated to secondary vertices

Table 2 Low-level and intermediate-level features for the neural network. The horizontal line separates low-level tracking and intermediate-level vertexing variables. These quantities are used for up to six tracks, ranked by signed transverse impact parameter significance. Vertex information is stored on a per-track level by utilizing a $N \rightarrow 1$ mapping. Adapted from Refs. [12, 59].

Short name	Description
Track d_0	impact parameter of the track, transverse to the beam line
Track z_0	impact parameter of the track, along the beam line
Track ϕ	azimuthal angle with respect to the beam axis
Track θ	polar angle with respect to the beam axis
Track Q/p	charge over momentum
Covariance between helix parameters	all 15 independent entries of the symmetric 5×5 covariance matrix between helix parameters of the track
Track weight	probability for a track to be associated with the primary vertex
Vertex mass	invariant mass of constituents used in secondary vertex fit
Vertex displacement	displacement of secondary vertex in transverse direction with respect to the interaction point
Vertex displacement significance	secondary vertex displacement divided by uncertainty of that displacement
N tracks	number of tracks associated to the secondary vertex
Vertex-Jet $\Delta\eta$	angular separation in η between jet axis and secondary vertex
Vertex-Jet $\Delta\phi$	angular separation in ϕ between jet axis and secondary vertex
Vertex energy fraction	fraction of jet energy carried by tracks associated to the secondary vertex